Environmental Research Communications

LETTER

First evidence for cold-adapted anaerobic oxidation of methane in deep sediments of thermokarst lakes

M Winkel[1,2,4] , A Sepulveda-Jauregui[1,4,5,6] , K Martinez-Cruz[1,5] , J K Heslop[1,7] , R Rijkers[2] , F Horn[2] , S Liebner[2,3] and K M Walter Anthony[1]

[1] Water and Environmental Research Center, Institute of Northern Engineering, University of Alaska, Fairbanks, United States of America
[2] GFZ German Research Centre for Geosciences, Helmholtz Centre Potsdam, section 3.7 Geomicrobiology, Potsdam, Germany
[3] University of Potsdam, Institute of Biochemistry and Biology, Potsdam, 14469, Germany
[4] These authors contributed equally to the work.
[5] Current address: University of Magallanes, Punta Arenas, Chile.
[6] Current address: Center for Climate and Resilience Research (CR)^2, University of Chile, Santiago, Chile.
[7] Current address: Department of Geography and Planning, Queens University, Kingston, Canada.

E-mail: mwinkel@gfz-potsdam.de

Abstract

Microbial decomposition of thawed permafrost carbon in thermokarst lakes leads to the release of ancient carbon as the greenhouse gas methane (CH_4), yet potential mitigating processes are not understood. Here, we report $\delta^{13}C–CH_4$ signatures in the pore water of a thermokarst lake sediment core that points towards *in situ* occurrence of anaerobic oxidation of methane (AOM). Analysis of the microbial communities showed a natural enrichment in CH_4-oxidizing archaeal communities that occur in sediment horizons at temperatures near 0 °C. These archaea also showed high rates of AOM in laboratory incubations. Calculation of the stable isotopes suggests that 41 to 83% of *in situ* dissolved CH_4 is consumed anaerobically. Quantification of functional genes (*mcrA*) for anaerobic methanotrophic communities revealed up to $6.7 \pm 0.7 \times 10^5$ copy numbers g^{-1} wet weight and showed similar abundances to bacterial 16S rRNA gene sequences in the sediment layers with the highest AOM rates. We conclude that these AOM communities are fueled by CH_4 produced from permafrost organic matter degradation in the underlying sediments that represent the radially expanding permafrost thaw front beneath the lake. If these communities are widespread in thermokarst environments, they could have a major mitigating effect on the global CH_4 emissions.

1. Introduction

Permafrost contains about 1307 Pg carbon (C), with a substantial amount (450 Pg C; >25% of thaw-susceptible C) found in the Yedoma regions (Walter Anthony *et al* 2014, Strauss *et al* 2017). Most of the C is stored in deep layers of undisturbed permafrost soils and organic-rich thermokarst (thaw) lake sediments (Strauss *et al* 2013, Walter Anthony *et al* 2014). Thermokarst lakes are estimated to cover 1.3×10^6 km^2 and store 102 Pg carbon (Olefeldt *et al* 2016). In the Northern Hemisphere, thermokarst lakes are hotspots of methane (CH_4) emission (Walter *et al* 2006) through multiple gas transport modes (Sepulveda-Jauregui *et al* 2015), and are estimated to emit 4.1 ± 2.2 Tg CH_4 per year (Wik *et al* 2016). Emissions from thermokarst lakes are expected to increase five-fold by 2100 (Schneider von Deimling *et al* 2015, Walter Anthony *et al* 2018). For better projections of CH_4 fluxes from high-arctic thermokarst lakes, we have to understand the molecular processes affecting CH_4 during its migration from deeper sediment layers to the atmosphere.

Evidence suggests a portion of CH_4 produced in thermokarst lakes is oxidized to the less potent greenhouse gas CO_2 prior to emission. A previous study of 30 Alaskan thermokarst lakes showed that aerobic CH_4 oxidation

takes place in the water column of lakes in the Yedoma region, and is significantly higher in Yedoma lakes than in non-Yedoma thermokarst lakes (Martinez-Cruz *et al* 2015). Aerobic methanotrophs have also been identified to oxidize CH_4 in near surface sediments (He *et al* 2012, Martinez-Cruz *et al* 2017). Even though the process of aerobic CH_4 oxidation seems to be wide spread in thermokarst lakes, little is known about the responsible microorganisms that control the CH_4 mitigation in the oxygenated lake habitats.

Notably, mitigating processes in the form of anaerobic oxidation of methane (AOM) in the deeper anoxic thermokarst lake talik (thaw bulb) sediments have not been previously studied. However, recent findings of AOM-related microorganisms in deep submarine permafrost point towards a potential role in similar habitats (Winkel *et al* 2018). Hitherto, there is only one study on AOM in permafrost (Winkel *et al* 2018) besides detection of sequences from anaerobic methanotrophic (ANME) (Kao-Kniffin *et al* 2015, Shcherbakova *et al* 2016) in permafrost environments. It is important to understand both aerobic and anaerobic oxidation of methane in this high methane emitting ecosystems to calculate fluxes and completely project C budgets that can be integrate it into new climate models.

AOM in marine environments is commonly performed by (ANME) archaea of the clades ANME-1a/b, $-2a/b$, $-2c$, and -3 (Ruff *et al* 2015). AOM is often coupled to sulfate reduction, hence ANME are found in consortia with deltaproteobacterial sulfate-reducing bacteria of the genera *Desulfococcus*, *Desulfosarcina*, or *Desulfobulbus* (Knittel and Boetius 2009). Beyond marine sediments the occurrence and activity of AOM performed through archaea has mainly been shown in anthropogenic influenced freshwater habitats (Raghoebarsing *et al* 2006, Vaksmaa *et al* 2016), while reports for pristine environments are rare (Schubert *et al* 2011. Gupta *et al* 2013, Timmers *et al* 2015, Weber *et al* 2017). In pristine, terrestrial environments, ANME of the GoM Arc I/AOM-associated archaea/ANME-2d lineage likely perform AOM. Genomes of this cluster originating from *Methanoperedens* spp. enrichments showed genes for denitrifying-driven (Haroon *et al* 2013) and iron-driven AOM (Ettwig *et al* 2016). Marker gene sequences of *Methanoperedenaceae* were also detected in permafrost environments (Kao-Kniffin *et al* 2015, Winkel *et al* 2018), but their activity remains to be proven.

To understand if CH_4 mitigation by AOM occurs in proximity of the permafrost thaw front at cold, near-zero temperatures, we sought AOM and the associated organisms by analyzing sediment samples from a depth profile in a well-characterized thermokarst lake, Vault Lake (Heslop *et al* 2015, Sepulveda-Jauregui *et al* 2015, Martinez-Cruz *et al* 2017). Sediment pore water CH_4 concentrations and $^{13}C–CH_4$ ratios were determined along a ~6 m sediment core, which extended through the talik into the underlying thawing permafrost. Further, we conducted potential AOM rate measurements of sediments using $^{13}C–CH_4$ isotopic tracer experiments and analyzed the *in situ* microbial community using 16S rRNA gene sequencing. We quantified anaerobic methanotrophic communities via quantitative PCR of the functional marker gene methyl-coenzyme M reductase, subunit alpha (*mcrA*) with specific primer for the *Methanoperedenaceae* cluster (Vaksmaa *et al* 2017). Additionally, ebullition bubbles emitted from the drilling boreholes and natural ebullition events were collected at Vault Lake and analyzed for CH_4 concentrations, isotopes ($\delta^{13}C–CH_4$ and δD), and radiocarbon age ($^{14}C–CH_4$).

2. Materials and methods

2.1. Sampling and physicochemical analysis

We collected ca. 6 m core from the center of Vault Lake (65.029 N°, 147.699 W°) during Spring 2013; a detailed description of the sampling procedure can be found in Heslop *et al* (2015). Studies of potential CH_4 production, biogeochemistry and soil organic carbon (SOC) quality from the same core were performed by Heslop and colleagues (2015). Briefly, Vault Lake is a thermokarst lake thought to have formed within the last 400 yr in a Yedoma-dominated region (Heslop *et al* 2015). Vault Lake is situated in an ecological area of northern boreal forest near Fairbanks, Alaska, USA, characterized by discontinuous permafrost. Limnologically, Vault Lake is considered a small shallow mixotrophic thermokarst lake with an area of 3,200 m^2, 3.7 m average depth, slightly alkaline, and black water (Heslop *et al* 2015, Sepulveda-Jauregui *et al* 2015). We collected sediment subsamples along the length of the core through the full talik profile, covering five major facies described by Heslop *et al* (2015): (i) organic-rich mud (0–152 cm), (ii) lacustrine silt (155–330 cm), (iii) taberite (331–508 cm), (iv) most recently-thawed taberite (509–555 cm), and (v) the transitional (thawing) permafrost (556–590 cm). We measured CH_4 concentration and $\delta^{13}C–CH_4$ in 38 core sediment subsamples. Several sections (20 samples) were used to explore potential AOM. Additionally, a few samples (5 samples) from representative horizons were used to analyze the microbial community via 16S rRNA gene sequencing (table S1 is available online at stacks.iop.org/ERC/1/021002/mmedia). Representative subsamples for each of the 5 different facies were analyzed for possible electron acceptors such as nitrate (detection limit ´dt´ 0.3 μM), nitrite (dt 0.03 μM), and sulfate (dt 1 μM) in pore water. Nitrate and nitrite were measured using a colorimetric technique (Clescerl *et al* 1999) while sulfate was measured with ion chromatography (ED40, Dionex, USA). We also analyzed sediment samples of a

CH$_4$ seep (Doughnut Lake) and a mud volcano (Obrien Pond) to explore how widespread CH$_4$ oxidation communities may be.

2.2. Concentration and stable isotope signatures of CH$_4$ measurements

CH$_4$ concentration and δ^{13}C–CH$_4$ ratios of pore water were measured from duplicate sediment plugs (n = 76) using a 5 ml polyethylene syringes with the end cut off, similar to Hoehler *et al* (2000). The 5 ml subsamples of sediment were immediately transferred into 20 ml serum vials containing 10 ml of CH$_4$ and CO$_2$-free water, closed with butyl rubber stoppers (Bellco) and aluminum crimp caps, and stored at $-8\,^{\circ}$C until their gas analysis to prevent oxygen interference.

In the laboratory, we thawed the subsamples at room temperature (21 $^{\circ}$C) then vigorously shook each serum vial for 60 s to reach equilibration between the slurry and the gas headspace. Total CH$_4$ concentration in the headspace was promptly measured by gas chromatography with a flame ionization detector (FID, Shimadzu GC-2014). Simultaneously, measurements of δ^{13}C–CH$_4$ ratios were determined by Cavity Ring-Down Spectroscopy (CRDS) using referenced standard of Vienna Pee Dee Belemnite-VPDB (G2201-i, Picarro, precision ± 0.55‰ δ^{13}VPDB for CH$_4$) coupled to a Small Sample Isotope Module (SSIM2, Picarro). SSIM2 was used to dilute the headspace samples with Zero Air. We determined CH$_4$ concentrations in the slurry using Henry's law following Sepulveda-Jauregui *et al* (2012). Henry's law constants for CH$_4$ at 298.15 K (1.4 10^{-3} mol L^{-1} Bar^{-1}) and its temperature dependence coefficient (2400 K) were determined according to Sepulveda-Jauregui *et al* (2012) using NIST database (2014). All CH$_4$ concentrations are expressed in micromolar concentrations.

2.3. Gas composition and isotopes from natural ebullition events and borehole bubbling

We directly collected natural ebullition event gas from both pockets of gas trapped in lake ice and from fresh ebullition events using submerged bubble traps placed near the surface of the water column above ebullition seeps. In addition to collecting gas from natural ebullition events, we collected four samples of free-phase ebullition bubbles emitted from the base of three boreholes drilled through the unfrozen sediments overlying permafrost at three separate locations (from the drilled sediment core, from a borehole directly next to the sediment core and one borehole from the margin of the lake) in Vault lake. These bubble samples rising from the base of the thaw bulb at 5.5, 7.0 and 8.8 m sediment depths in the three boreholes were collected using submerged umbrella-style traps deployed directly below the lake water surface above the boreholes. All bubble gas was collected into 20-ml or 60-ml glass serum vials. CH$_4$ and CO$_2$ concentrations were measured as described previously (Walter Anthony *et al* 2016). Radiocarbon age of CH$_4$ was determined in a subset of the lake bubble samples by the ^{14}C/^{12}C isotopic ratio of CH$_4$ following methods described previously (Walter Anthony *et al* 2016).

2.4. Anaerobic oxidation of methane (AOM) stable isotope incubation

We estimated the potential AOM using incubations of core subsamples from 20 depths. Subsamples were diluted (1:1 v/v) in triplicate with sterile, CH$_4$ and CO$_2$-free anaerobic distilled water. Briefly, we transferred 50 ml of the slurry to 100 ml serological bottles under continuous flushing with ultra-high purity (UHP) N$_2$ (Air Liquide, Houston, TX, USA). After 5 minutes of additional flushing, the serological vials were sealed with blue butyl rubber stoppers (Bellco) and crimped with aluminum caps. We injected L-cysteine in each vial to a concentration of 0.025% to reduce anoxic media. Each vial was pre-incubated for five days to ensure the absence of oxygen, which we also confirmed by headspace measurement using a gas chromatograph equipped with a thermal conductivity detector (Shimadzu GC-2014). After pre-incubations, we added 2 ml of ^{13}CH$_4$ (99 atom % ^{13}C, Sigma Aldrich) to the headspace of each incubation vial. We determined potential AOM rates as previously described by (Beal *et al* 2009, Blazewicz *et al* 2012). The concentrations of ^{13}C–CH$_4$ were determined from the isotopic fractions and the total CH$_4$ concentration determined by gas chromatography (described in above section). For our calculations, AOM was conservatively determined from ^{13}C–CH$_4$ oxidation. We calculated AOM rates from the linear decrease against time (ca. 200 days) in ^{13}C–CH$_4$.

2.5. DNA extraction, 16S rRNA gene Illumina HiSeq sequencing and analysis

We extracted genomic DNA of 4.7–13 g sediment using procedures described in Zhou *et al* (1996). Afterwards, we quantified DNA concentrations with Nanophotometer$^{\circledR}$ P360 (Implen GmbH) and Qubit$^{\circledR}$ 2.0 Flurometer (Thermo Fisher Scientific).

Amplification of bacterial and archaeal 16S rRNA genes, were performed separately for a better depth resolution of archaea and have been described previously (Winkel *et al* 2018). Briefly, we amplified bacteria with the primer combination S-D-Bact-0341-a-S-17 and S-D-Bact-0785-a-A-21. Archaea were amplified with a nested PCR using the primer S-D-Arch-0020-a-S-19 and S-D-Arch-0958-a-A-19 for the first PCR with 40 cycles

and S-D-Arch-0349-a-S-17 and S-D-Arch-0786-a-A-20 for the second PCR with 35 cycles, respectively. All PCR conditions can be found in Winkel *et al* (2018). We pooled 3 individual PCR products per sample to reduce the bias. We pooled equimolar concentrations of PCR products from each sample for the sequencing run. Archaeal and bacterial runs included positive controls (*Escherichia coli* and *Methanobacterium lacus*) and negative PCR controls to estimate a sequencing run error.

Sequencing was performed on an Illumina HiSeq 2500 sequencer using the HiSeq Rapid Run 300 bp PE sequencing mode (GATC Biotech, Germany). The library was prepared with the MiSeq Reagent Kit V3 for 2×300 bp paired-end reads. To introduce sequence diversity in this low-complexity library, 20% PhiX control v3 library was used.

We used a customized QIIME pipeline to analyze the quality and taxonomic classification of the sequences as described previously (Winkel *et al* 2018). Briefly, the quality of the sequences was analyzed with the fastqc tool (http://bioinformatics.babraham.ac.uk/projects/fastqc/ by S Andrews). Raw reads of sequences were de-multiplexed and barcodes were removed with the CutAdapt tool (Martin 2011). The subsequent steps included merging of reads using overlapping sequence regions using PEAR (Zhang *et al* 2014), standardizing the orientation of the nucleotide sequence, and trimming and filtering sequences with low quality by Trimmomatic (Bolger *et al* 2014). All parameters are the same as described previously (Winkel *et al* 2018). Subsequently, we clustered sequences into operational taxonomic units (OTUs) at a nucleotide cutoff level of 97% similarity and taxonomically assigned employing the Silva database release 128 (Quast *et al* 2012) using the pick_open_reference approach of the QIIME pipeline (Caporaso *et al* 2010). Singletons, chloroplasts and mitochondrial sequences were excluded from the OTU table. Older taxonomic assignments for archaea and bacteria were corrected manually after (Rinke *et al* 2013, Castelle *et al* 2015, Adam *et al* 2017) e.g. Miscellaneous Crenarchaeal Group (MCG) was renamed to *Bathyarchaeota*. OTUs with relative abundance lower than 0.1% for the individual libraries were not analyzed.

2.6. Quantification of bacterial 16S rRNA genes, ANME-2d *mcrA* and methanogens *mcrA*

Diluted DNA (1:1000) was used to eliminate inhibition effects in the quantitative PCR. Quantitative PCR has been described previously (Winkel *et al* 2018). Briefly, we amplified bacterial 16S rRNA genes, methanogenic *mcrA* and specific ANME-2d *mcrA* by primer combinations found in table S2. The PCR reagents and conditions are described in (Winkel *et al* 2018). For standards we used cloned products of know size and concentrations. Specificity of the PCR products were checked by a melt analysis against products of the standard. The efficiency of the qPCR varied between 90 and 100% and the R^2 values of the standard dilutions (5 serial dilutions in triplicates) was 0.996.

2.7. Calculating of CH_4 fraction that got oxidized based on $^{13}C–CH_4$ changes

We used highest changes in stable isotope signatures of dissolved CH_4 in the cores to calculate the fraction of produced CH_4 that got oxidized ($f_{ox,i}$). Therefore we used equation after Liptay *et al* (1998):

$$f_{ox,i} = \frac{\delta_o - \delta_p}{1000 * (\propto_{ox} - \propto_{trans})}$$

where δ_o and δ_p are the $\delta^{13}C$ values (in ‰) of CH_4 in different horizons of the taberite layers. α_{ox} and α_{trans} are fractionation factors for AOM and CH_4 transport, respectively. Percentage of oxidized CH_4 is than calculated. ($f_{ox} \times 100$).

We assumed CH_4 to be transported mainly by diffusion and therefore used a soil fractionation factor of $\alpha_{trans} = 1.001$ after Preuss *et al* (2013). Different fractionation factors (α_{ox}) for AOM in freshwater system were used mainly for sulfate-dependent AOM ($\alpha_{ox} = 1.031$) (Schubert *et al* 2011), iron-dependent AOM ($\alpha_{ox} = 1.030$) (Norði *et al* 2013), and nitrate-dependent AOM ($\alpha_{ox} = 1.032$) (Norði and Thamdrup 2014).

3. Results

3.1. Pore water and bubble methane analysis

Radiocarbon dating of CH_4-rich bubbles from the borehole that reflects the transitional permafrost (mean CH_4: 79.82 ± 24.8%, CO_2: 0.81 ± 1.1%) revealed a C age of 21.1 ± 0.08 kyr, in comparison to CH_4 of bubbles from natural ebullition events (mean CH_4: 73.6 ± 23.1%, CO_2: 0.53 ± 0.4%) that showed a mixture of old and young carbon (mean: 9.7 kyr, range 2.2–28.5 kyr table 1).

$\delta^{13}C–CH_4$ and δD-CH_4 values of gas bubbles (n = 4) emitted from the base of the drilling boreholes (e.g. transitional permafrost facie) were highly depleted (-72.7 ± 4.4‰ and -390.4 ± 16.0‰, respectively, table 1). Bubbles collected from natural ebullition events showed slightly enriched $\delta^{13}C–CH_4$ values
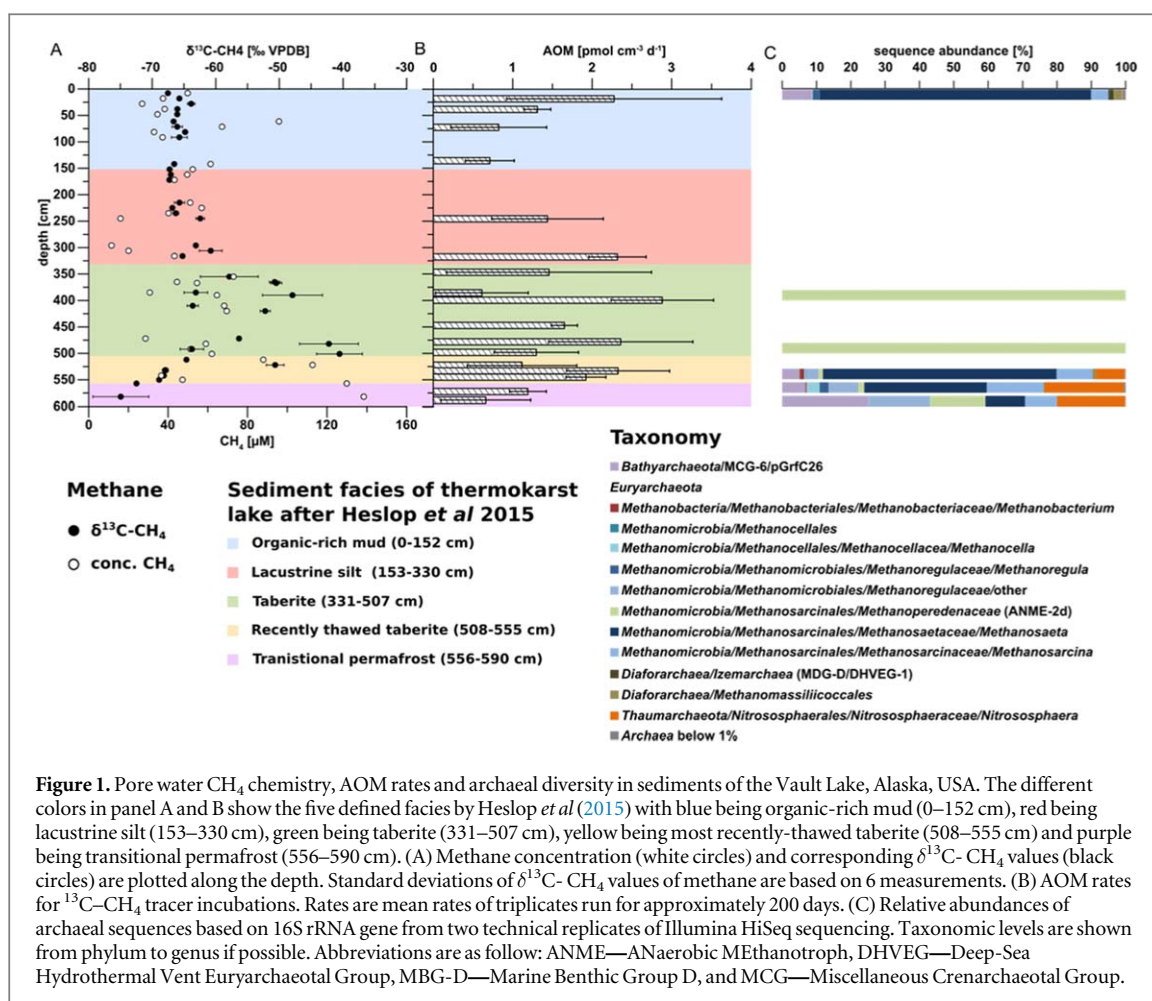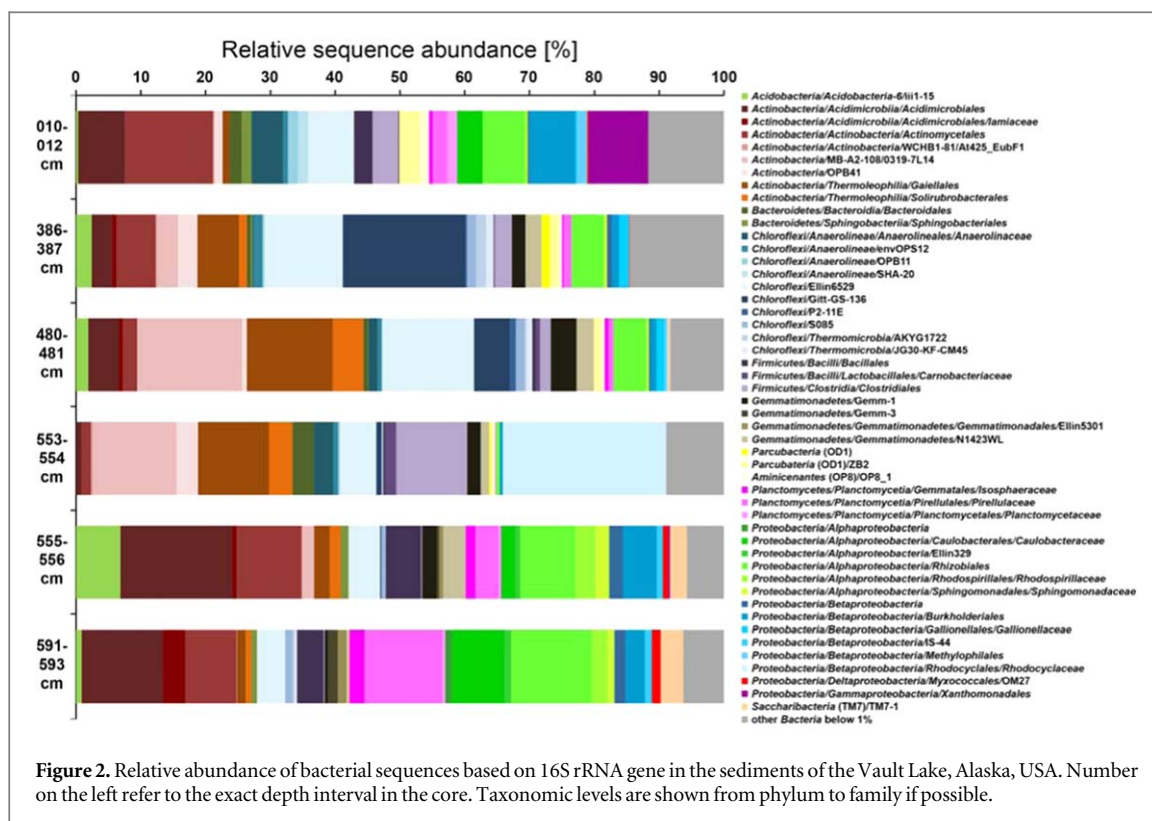
Figure 1. Pore water CH_4 chemistry, AOM rates and archaeal diversity in sediments of the Vault Lake, Alaska, USA. The different colors in panel A and B show the five defined facies by Heslop *et al* (2015) with blue being organic-rich mud (0–152 cm), red being lacustrine silt (153–330 cm), green being taberite (331–507 cm), yellow being most recently-thawed taberite (508–555 cm) and purple being transitional permafrost (556–590 cm). (A) Methane concentration (white circles) and corresponding $\delta^{13}C$- CH_4 values (black circles) are plotted along the depth. Standard deviations of $\delta^{13}C$- CH_4 values of methane are based on 6 measurements. (B) AOM rates for $^{13}C–CH_4$ tracer incubations. Rates are mean rates of triplicates run for approximately 200 days. (C) Relative abundances of archaeal sequences based on 16S rRNA gene from two technical replicates of Illumina HiSeq sequencing. Taxonomic levels are shown from phylum to genus if possible. Abbreviations are as follow: ANME—ANaerobic MEthanotroph, DHVEG—Deep-Sea Hydrothermal Vent Euryarchaeotal Group, MBG-D—Marine Benthic Group D, and MCG—Miscellaneous Crenarchaeotal Group.

Table 1. Composition of CO_2, CH_4 and N_2 in gas bubbles and isotopic signatures of CH_4.

	Natural ebullition events			Bubbles released from deep boreholes following drilling		
	mean	stdev	n	mean	stdev	n
CO_2 (%)	0.53	0.38	35	0.81	1.12	9
CH_4 (%)	73.61	23.11	35	79.82	24.79	9
N_2 (%)	25.40	22.43	23	12.72	8.26	5
$\delta^{13}C$ CH_4 (‰)	−67.67	3.42	20	−72.67	4.35	4
δD CH_4 (‰)	−382.90	12.43	20	−390.41	15.96	4
$^{14}C–CH_4$ (fM)	0.30	0.26	9	0.07		1
$^{14}C–CH_4$ (yrs BP)	9,715	2,190–28,500[a]	9	21,068	80	1

[a] The range of $^{14}C–CH_4$ measurements for natural ebullition events was given to account for the large variability.

(−67.7 ± 3.4‰) but were still highly depleted in δD-CH_4 (−382.9 ± 12.4‰, table 1). Mean values are plotting in the mixed zone of microbial methane production (figure S1).

The transitional permafrost, located at the base of the radially expanding talik directly above the thaw boundary, showed the highest *in situ* sediment pore water CH_4 concentrations (mean 134 ± 8 μM) with depleted $\delta^{13}C–CH_4$ between −75‰ and −73‰ (figure 1(a)), similar to borehole methane values. The recently-thawed taberite showed a slight enrichment in $\delta^{13}C–CH_4$ (−69 to −50‰) and a decrease in CH_4 concentration (figure 1(a)). In striking contrast, the taberite layers, located above the recently-thawed taberite, were characterized by large $\delta^{13}C–CH_4$ fractionation (−63 to −40‰) and low CH_4 concentrations (down to 28 μM, figure 1(a)). Based on the range of AOM fractionation factors (1.030–1.032, Schubert *et al* 2011, Norði *et al* 2013, Norði and Thamdrup 2014) reported for freshwater systems, our calculations (Liptay *et al* 1998) of large isotopic changes (becoming more enriched in $\delta^{13}C–CH_4$) - expecting CH_4 to diffuse upwards - suggested that 41% to

Figure 2. Relative abundance of bacterial sequences based on 16S rRNA gene in the sediments of the Vault Lake, Alaska, USA. Number on the left refer to the exact depth interval in the core. Taxonomic levels are shown from phylum to family if possible.

83% of the *in situ* CH$_4$ fraction in the taberite and upper recently-thawed taberite layers (311 to 532 cm, figure 1(a)) got oxidized. With a few exception (right above the taberite), CH$_4$ concentration in the lacustrine and organic-rich facie scattered around $43 \pm 19\ \mu$M with δ^{13}C–CH$_4$ of -65.5 ± 1.8‰ (figure 1(a)).

3.2. Potential AOM rates and possible electron acceptors

Our ^{13}C–CH$_4$ tracer incubations showed low AOM rates in the transitional permafrost (~ 0.9 pmol cm^{-3} d^{-1}) that doubled in the recently-thawed taberite. Even though potential AOM rates were scattered, we observed the highest rates for the whole core in the taberite layer (up to 2.88 pmol cm^{-3} d^{-1}; mean 1.7 ± 0.7 pmol cm^{-3} d^{-1}, figure 1(b)). Potential AOM rates decreased towards the surface of the core but started to increase again above 100 cm, and showed 2.3 pmol cm^{-3} d^{-1} in the upper most surface sample (figure 1(b)).

Nitrate concentrations in all taberite layers were below the detection limit ($<0.3\ \mu$M), and only measurable in the lacustrine and organic-rich facies ($39.8 \pm 30.5\ \mu$M and $58.2 \pm 3.7\ \mu$M, respectively). Interestingly, the concentration of nitrite increased just above the transitional permafrost (554.4 cm) showing extremely high *in situ* concentration ($\sim 660\ \mu$M) in the transitional permafrost. Sulfate showed extremely high concentration (up to 35 ± 2 mM) in the taberite layers and also showed high concentrations (3 ± 0.2 mM) in the surface facie (table S4).

3.3. Microbial community structure

Microbial community analyses revealed high archaeal diversity (highest invers Simpson 6.33 to 7.90, table S3) at the permafrost thaw front (i.e. transitional permafrost and base of recently-thawed taberite) that cluster together with archaeal community of the surface sediment (figure S2(a)) and included many representative OTUs related to methanogens (*Methanosaeta* 12%–68%, *Methanosarcina* 9%–16%, and *Methanoregulaceae* 3%–18%). The transitional permafrost showed the highest occurrence of *Planctomycetes* sequences of all bacterial communities (figure 2). Other bacterial sequences fell into dominant taxa of *Alphaproteobacteria* (*Caulobacteraceae, Rhizobiales, Rhodospirillaceae, Sphingomonadace*), *Betaproteobacteria* (*Burkholderiales*), *Saccharibacteria* (TM7), *Firmicutes* (*Bacillales*), *Actinobacteria* (*Actinomycetales, Acidimicrobiales*), and *Chloroflexi* (Ellin6529). The bacterial communities of the transitional permafrost cluster together with most surface sample (10–20 cm) (figure S2(b)). In contrast to the archaea, the bacterial communities of all taberite layers cluster together (figure S2(b)) and show an increase in taxa of *Betaproteobacteria (Rhodocyclaceae/Dechloromonas)* and different *Firmicutes*. For detailed microbial descriptions, please see the supplementary information.

The archaeal communities of the taberite layer cluster together were almost exclusively represented by ANME-2d sequence of the *Methanoperedenaceae* (figure 1(c)). Phylogenetic analysis of the
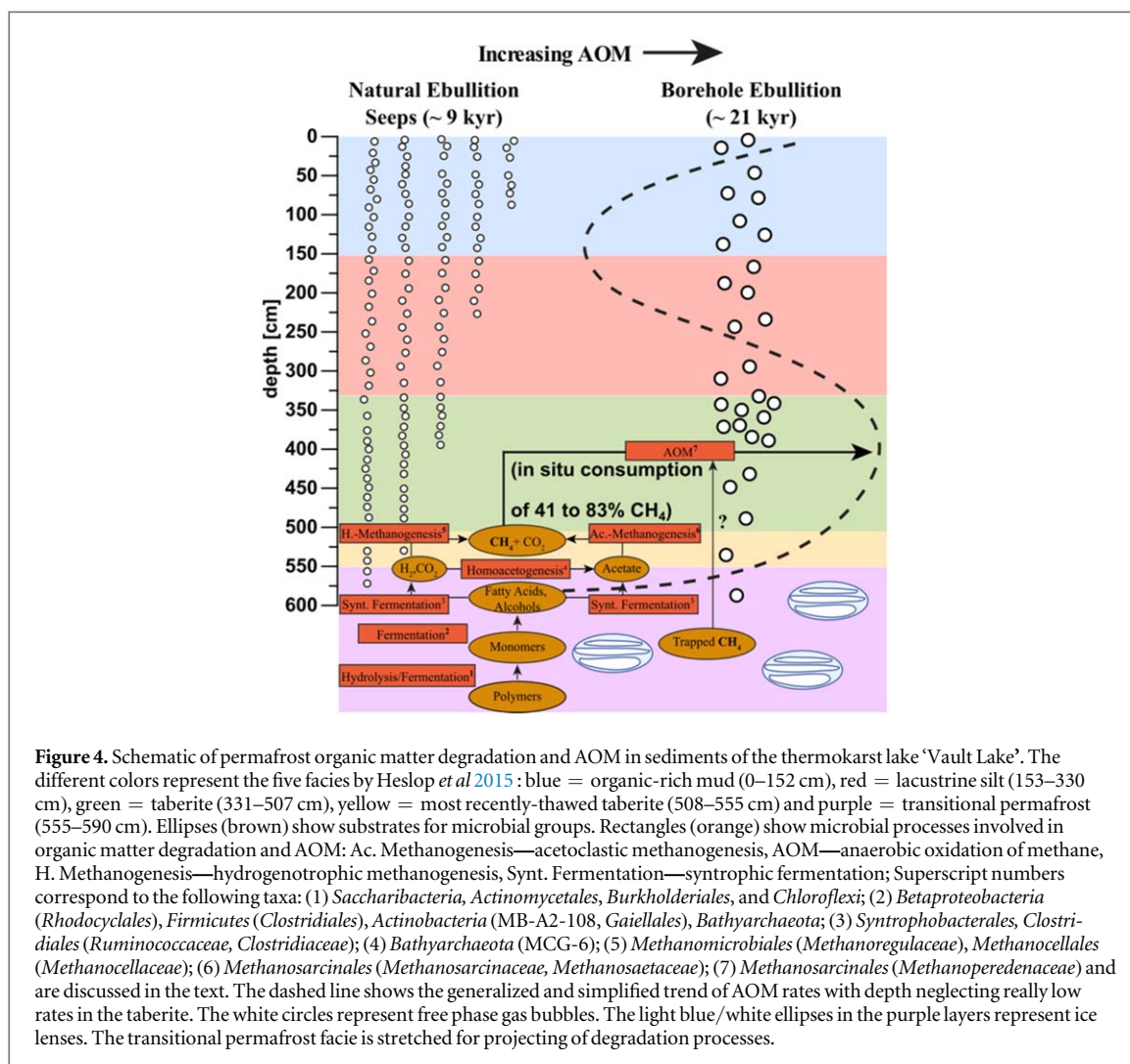
Figure 3. Phylogenetic affiliation of *Methanoperedenaceae*-related sequences based on 16S rRNA gene. OTUs from the Vault Lake are shown in bold black. Reference sequences are colored coded relating to their detected habitat. *Methanopyrus kandleri* was used as outgroup. Boot-strap values at inner nodes are given by >90% (black circle), >70% (gray circle), and >50% (white circle). The scale bar represents 10 percent sequence divergence.

Methanoperedenaceae-related OTUs showed an affiliation with two different freshwater clusters (figure 3) mainly comprised of sequences from lake, river, permafrost, iron-rich mat habitats and a *Methanoperedens* sp. that uses nitrate and iron as electron acceptor (Ettwig *et al* 2016). Quantification of *Methanoperedenaceae* (ANME-2d) using specific primers for their functional *mcrA*, revealed $5.7–6.7 \times 10^5 \pm 0.7–1 \times 10^5$ copy numbers g^{-1} wet weight. While bacterial 16S rRNA gene copy numbers in the taberite layer showed similar values (table S2), methanogenic *mcrA* copy numbers were below the detection limit ($<10^2$ copy numbers g^{-1} wet weight, table S5) and methanogenic 16S rRNA sequencing revealed only poor contribution to the overall archaeal abundance ($<0.02\%$). Additional analysis of a methane seep and a mud volcano from two other lakes revealed a low abundance ($\sim1\%$) of *Methanoperedenaceae* sequences (figure S3).

4. Discussion

Vault Lake is a thermokarst lake in the discontinuous permafrost region near Fairbanks Alaska, USA. It is a typical first generation thermokarst lake formed by melting of permafrost ground ice. It has massive ice wedges (figure 4), and steep eroding bluffs and several CH_4 seeps that indicate actively deepening. Radiocarbon dating from borehole ebullition clearly reveals a Pleistocene age (~ 21 kyr) of C–CH_4 falling into the typical range of point sources from thermokarst lakes (Walter *et al* 2007). In contrast, the age of natural ebullition seeps showed a mixture (2 to 28 kyr) of different ages most likely reflecting the production from different aged C sources and,

Figure 4. Schematic of permafrost organic matter degradation and AOM in sediments of the thermokarst lake 'Vault Lake'. The different colors represent the five facies by Heslop *et al* 2015 : blue = organic-rich mud (0–152 cm), red = lacustrine silt (153–330 cm), green = taberite (331–507 cm), yellow = most recently-thawed taberite (508–555 cm) and purple = transitional permafrost (555–590 cm). Ellipses (brown) show substrates for microbial groups. Rectangles (orange) show microbial processes involved in organic matter degradation and AOM: Ac. Methanogenesis—acetoclastic methanogenesis, AOM—anaerobic oxidation of methane, H. Methanogenesis—hydrogenotrophic methanogenesis, Synt. Fermentation—syntrophic fermentation; Superscript numbers correspond to the following taxa: (1) *Saccharibacteria, Actinomycetales, Burkholderiales*, and *Chloroflexi*; (2) *Betaproteobacteria* (*Rhodocyclales*), *Firmicutes* (*Clostridiales*), *Actinobacteria* (MB-A2-108, *Gaiellales*), *Bathyarchaeota*; (3) *Syntrophobacterales, Clostridiales* (*Ruminococcaceae, Clostridiaceae*); (4) *Bathyarchaeota* (MCG-6); (5) *Methanomicrobiales* (*Methanoregulaceae*), *Methanocellales* (*Methanocellaceae*); (6) *Methanosarcinales* (*Methanosarcinaceae, Methanosaetaceae*); (7) *Methanosarcinales* (*Methanoperedenaceae*) and are discussed in the text. The dashed line shows the generalized and simplified trend of AOM rates with depth neglecting really low rates in the taberite. The white circles represent free phase gas bubbles. The light blue/white ellipses in the purple layers represent ice lenses. The transitional permafrost facie is stretched for projecting of degradation processes.

therefore, ebullition from different sediment depths (figure 4) falling into the range of background and point sources (Walter *et al* 2007).

Bubbles from the borehole showed highly depleted δ^{13}C–CH$_4$ and δD that point towards biological CH$_4$ production (Whiticar 1999). Even though δ^{13}C–CH$_4$ values indicate hydrogenotrophic methanogenesis, the highly depleted δD values are atypical and might indicate an unusual substrate (e.g. short chain alkanes, Borrel *et al* 2019), be an effect of higher partial pressure (Bilek *et al* 2001), or reflect a different methanogenic pathway (e.g. methylotrophic methanogenesis, Sorokin *et al* 2017). Pore water CH$_4$ from the transitional permafrost, which reflects ice-bearing sediments with a large quantity of unfrozen water in the inter-pore space, had similar δ^{13}C–CH$_4$ values to the borehole ebullition gas. Since the transitional permafrost also showed the highest CH$_4$ concentration, it indicates that this might be a horizon of high *in situ* CH$_4$ production due to degrading permafrost providing methanogens with substrates. Another possible explanation might be that previously produced CH$_4$ was entrapped during permafrost formation in the Pleistocene and released through thawing. However, based on the cold, dry steppe conditions during Yedoma formation at this site (Heslop *et al* 2015) and low abundance of methanogens in undisturbed Yedoma sediments (Bischoff *et al* 2013, Rivkina *et al* 2016), we interpret the high concentrations of pore water dissolved CH$_4$ to be the result of present-day methanogenesis at the thaw front. The depleted δ^{13}C–CH$_4$ showed similar δ^{13}C–CH$_4$ values (−70.9 to −73‰) to hydrogenotrophic methanogenesis of peatlands (Avery *et al* 1999, Galand *et al* 2010, McCalley *et al* 2014), however, missing δD values from the pore water analysis prevents further interpretation in comparison to methane from the borehole bubbles.

Moving from the transitional permafrost towards recently-thawed taberite, the archaeal community had increasing proportions of methanogens supporting recently found CH$_4$ production in the same sediment layers (Heslop *et al* 2015). CH$_4$ production occurred most likely from precursors such as acetate and formate as well as H$_2$/CO$_2$. Acetate and formate are known to occur in high concentration in Pleistocene sediments (Strauss *et al*

2015, Mitzscherling *et al* 2017), especially in Yedoma regions (Ewing *et al* 2016). CO_2 concentrations measured at the same depth showed values between 120 to 1000 mM (A. Sepulveda-Jauregui, unpublished data). Some bacterial taxa (*Planctomycetes and Alphaproteobacteria*) in the transitional permafrost, which are often found in peatlands, can be related to aerobic lifestyles and could point to relicts from conditions during the Pleistocene, while many taxa such as *Burkholderiales, Saccharibacteria, Myxococcales, Actinomycetales,* and *Chloroflexi* are related to species that are known to anaerobically hydrolyze plant polymers as the first step of organic matter degradation (figure 4). Interestingly, the bacterial communities of the transitional permafrost cluster together with the sample nearest to the surface (10–20 cm, figure S2(b)) that are influenced by fresh organic matter input from lake primary production during summer (Martinez-Cruz *et al* 2015).

The slight increase in $\delta^{13}C$–CH_4 values in the pore water CH_4 in the recently-thawed taberite might be due to availability of other substrates such as acetate and could also explain the increase in *Methanosaeta* (figure 1(c)), which solely uses acetate as substrate (Michał *et al* 2018). In all taberite layers, we also detected an increase in bacterial groups that are known fermenters (*Betaproteobacteria/Rhodocyclaceae/Dechloromonas, Firmicutes/Clostridiales*) and syntrophs (*Ruminococcaceae, Syntrophobacterales, Clostridiaceae*) known to degrade monomers into acetate, hydrogen, carbon dioxide, and formate as precursors for CH_4 production (figure 4). Compared to organic decomposition processes in typical active layers (Tveit *et al* 2012), where fresh material is broken into polymers and monomers and then hydrolyzed and fermented into methanogenic precursors with depth, permafrost organic matter in thermokarst lake talik is decomposed by metabolic processes that occur in the inverse depth order (figure 4). For detailed microbial descriptions, please see the supplementary information.

The taberite facies also showed the most fractionated $\delta^{13}C$–CH_4, with enriched CH_4 up to 40‰ pointing towards oxidation (Whiticar 1999) and reaching similar values as reported for AOM in other freshwater sediments (Schubert *et al* 2011, Norði *et al* 2013, Norði and Thamdrup 2014). Our calculated fraction of CH_4 that was oxidized in the taberite facie is consistent with previously reported CH_4 measurements and isotopic values from other Alaskan lakes that also assumed CH_4 oxidation, but were mainly attributed to aerobic oxidation (Elder *et al* 2018). Our highest measured potential AOM rates in the taberite suggests this layer is a hotspot for AOM. The archaeal sequence analysis supports this findings as we almost exclusively found *Methanoperedenaceae* known for nitrate-driven (Haroon *et al* 2013) or iron-driven AOM (Ettwig *et al* 2016, Cai *et al* 2018). To rule out any sequencing artifact, we analyzed the quantity of the functional *mcrA*, which revealed similar copy numbers to the entire bacterial community and were in the range of river sediments (Vaksmaa *et al* 2016). Methanogens in this horizon were below the detection limit ($<10^2$ copy numbers), even though long-term incubations (>115 days) indicated a reactivation of methanogens (Heslop *et al* 2015). Measurements for potential electron acceptors revealed no detectable nitrate, in the taberite layers, which might indicate low concentrations in the pore water that could not support AOM or high turnover of nitrate. Interestingly, high nitrite concentrations in the interface of transitional and recently-thawed permafrost could point towards incomplete denitrification of AOM, since *Methanoperedenaceae* sequences were also found in lower abundances in these layers (figure 1(c)). We also detected unusually high sulfate concentrations in the taberite, while potential sulfate-reducing microorganisms were low in abundance (up to 0.7% relative abundance, data not shown). It is therefore not clear if sulfate is used as electron acceptor coupled to AOM. Other electron acceptors for AOM in freshwater sediments are metal oxides of iron (Weber *et al* 2017) and manganese that could support Fe(III)-dependent AOM (Ettwig *et al* 2016, Cai *et al* 2018). No pore water iron concentration or reactive iron solid phases have been measured for the Vault Lake sediment. However, pore water measurements in other thermokarst lakes showed high Fe(III) concentrations at the thaw boundary (Winkel, unpublished data). Therefore, iron could be involved in AOM by *Methanoperedenaceae*, as recently been shown (Ettwig *et al* 2016, Cai *et al* 2018), and might play a role in deeper sediments (Egger *et al* 2015).

Potential AOM rates decreased moving towards the surface of the core but started to increase again at 100 cm depth (figure 1(b)), pointing towards a second zone of AOM in near-surface sediments (generalized dashed line, figure 4). AOM activity in surface sediment layers of the Vault Lake was recently ascribed by Martinez-Cruz and colleagues (Martinez-Cruz *et al* 2017) to an entirely different microbial community, namely aerobic methanotrophs consuming CH_4 under anaerobic conditions. Our data support this hypothesis, since we did not find any ANME or NC10 phylum microorganisms (Ettwig *et al* 2010) that would support a typical AOM community but found low abundances of aerobic methanotrophs (*Crenotrichaceae, Methylophilaceae* and *Methylocystaceae*) similar to Martinez-Cruz and colleagues (Martinez-Cruz *et al* 2017). However, presently undiscovered anaerobic methanotrophs could also be responsible for the second AOM peak. The $\delta^{13}C$–CH_4 (mean -65.5 ± 1.8‰) in the lacustrine silt and organic-rich mud facies were similar to the natural ebullition event bubbles, despite a few layers with low (lacustrine silt) or high concentrations (organic-rich mud).

5. Conclusions

We found that AOM occurs in thermokarst lake sediments and mitigates diffusive CH_4 emission from these lakes. Previous work suggests that CH_4 primarily escapes from talik sediments as bubbles through secondary pore channels (i.e. bubble tubes) (Sepulveda-Jauregui *et al* 2015). This is largely due to low hydraulic conductivity of the silt-dominated Yedoma sediments, which inhibits diffusion of dissolved CH_4 and therefore traps dissolved CH_4 in the sediment pore water where it is subject to anaerobic microbial oxidation. As a result, *Methanoperedenaceae* anaerobically oxidize CH_4 at rates similar to other lake sediments (Knittel and Boetius 2009) effectively filtering for dissolved CH_4 concentrations despite the near 0 °C temperature conditions. Recent findings on AOM in degrading submarine permafrost that also showed natural enrichments in *Methanoperedenaceae*-related communities (Winkel *et al* 2018) support the findings of cold-adapted anaerobic methanotrophic communities. *Methanoperedenaceae* in thermokarst lakes were mainly found in deep sediment layers and mud volcanos that represents windows to the subsurface (Ruff *et al* 2018). AOM in thermokarst lake sediments may play an important role in mitigating the release of ancient CH_4 as permafrost warms and thaws beneath lakes (Walter Anthony *et al* 2018). Since our analyses were done on one sediment core and the study lacks certain chemical and physical background data, additional thermokarst lakes need to be investigated in the future to understand if such a mitigation process along the deep permafrost thaw front is widespread. In particular, what kind of electron acceptor is used in the process of AOM should be studied to understand the molecular process in freshwater thermokarst lake environments with many possible electron acceptors such as metal oxides, nitrate and humic acids.

ORCID iDs

M Winkel ⦿ https://orcid.org/0000-0003-3692-0952
A Sepulveda-Jauregui ⦿ https://orcid.org/0000-0001-7777-4520
K Martinez-Cruz ⦿ https://orcid.org/0000-0001-9365-0616
J K Heslop ⦿ https://orcid.org/0000-0002-8243-4456
R Rijkers ⦿ https://orcid.org/0000-0001-7263-8917
F Horn ⦿ https://orcid.org/0000-0002-4070-3400
S Liebner ⦿ https://orcid.org/0000-0002-9389-7093
K M Walter Anthony ⦿ https://orcid.org/0000-0003-2079-2896

References

Adam P S, Borrel G, Brochier-Armanet C and Gribaldo S 2017 The growing tree of Archaea: new perspectives on their diversity, evolution and ecology *ISME J.* **11** 2407–2425

Avery G B, Shannon R D, White J R, Martens C S and Alperin M J 1999 Effect of seasonal changes in the pathways of methanogenesis on the δ13C values of pore water methane in a Michigan peatland *Glob. Biogeochem. Cycles* **13** 475–84

Beal E J, House C H and Orphan V J 2009 Manganese- and iron-dependent marine methane oxidation *Science* **325** 184–7

Bilek R S, Tyler S C, Kurihara M and Yagi K 2001 Investigation of cattle methane production and emission over a 24-hour period using measurements of δ13C and δD of emitted CH4 and rumen water *J. Geophys. Res. Atmospheres* **106** 15405–13

Bischoff J, Mangelsdorf K, Gattinger A, Schloter M, Kurchatova A N, Herzschuh U and Wagner D 2013 Response of methanogenic archaea to Late Pleistocene and Holocene climate changes in the Siberian *Arctic Glob. Biogeochem. Cycles* **27** 305-317

Blazewicz S J, Petersen D G, Waldrop M P and Firestone M K 2012 Anaerobic oxidation of methane in tropical and boreal soils: ecological significance in terrestrial methane cycling *J. Geophys. Res. Biogeosciences* **117** G02033

Bolger A M, Lohse M and Usadel B 2014 Trimmomatic: a flexible trimmer for Illumina sequence data *Bioinformatics* **30** 2114–20

Borrel G *et al* 2019 Wide diversity of methane and short-chain alkane metabolisms in uncultured archaea *Nat. Microbiol.* **4** 603–13

Cai C, Leu A O, Xie G-J, Guo J, Feng Y, Zhao J-X, Tyson G W, Yuan Z and Hu S 2018 A methanotrophic archaeon couples anaerobic oxidation of methane to Fe(III) reduction *ISME J.* **12** 1929–39

Caporaso J G *et al* 2010 QIIME allows analysis of high-throughput community sequencing data *Nat. Methods* **7** 335–6

Castelle C J *et al* 2015 Genomic expansion of domain archaea highlights roles for organisms from new phyla in anaerobic carbon cycling *Curr. Biol.* **25** 690–701

Clescerl L S, Greenberg A E and Eaton A D 1999 *Standard Methods for Examination of Water & Wastewater* (Washington: Amer Public Health Assn)

Egger M *et al* 2015 Iron-mediated anaerobic oxidation of methane in brackish coastal sediments *Environ. Sci. Technol.* **49** 277–83

Elder C D, Xu X, Walker J, Schnell J L, Hinkel K M, Townsend-Small A, Arp C D, Pohlman J W, Gaglioti B V and Czimczik C I 2018 Greenhouse gas emissions from diverse Arctic Alaskan lakes are dominated by young carbon *Nat. Clim. Change* **8** 166–71

Ettwig K F *et al* 2010 Nitrite-driven anaerobic methane oxidation by oxygenic bacteria *Nature* **464** 543–8

Ettwig K F, Zhu B, Speth D, Keltjens J T, Jetten M S M and Kartal B 2016 Archaea catalyze iron-dependent anaerobic oxidation of methane *Proc. Natl Acad. Sci.* **113** 12792–6

Ewing S, O'Donnell Jonathan A, Aiken George R, Kenna B, David B, Windham-Myers L and Kanevskiy Mikhail Z 2016 Long-term anoxia and release of ancient, labile carbon upon thaw of Pleistocene permafrost *Geophys. Res. Lett.* **42** 10730–8

Galand P E, Yrjälä K and Conrad R 2010 Stable carbon isotope fractionation during methanogenesis in three boreal peatland ecosystems *Biogeosciences* **7** 3893–900

Gupta V, Smemo K A, Yavitt J B, Fowle D, Branfireun B and Basiliko N 2013 Stable isotopes reveal widespread anaerobic methane oxidation across latitude and peatland type *Environ. Sci. Technol.* **47** 8273–9

Haroon M F, Hu S, Shi Y, Imelfort M, Keller J, Hugenholtz P, Yuan Z and Tyson G W 2013 Anaerobic oxidation of methane coupled to nitrate reduction in a novel archaeal lineage *Nature* **500** 567–70

He R, Wooller M J, Pohlman J W, Quensen J, Tiedje J M and Leigh M B 2012 Diversity of active aerobic methanotrophs along depth profiles of arctic and subarctic lake water column and sediments *ISME J.* **6** 1937–48

Heslop J K, Walter Anthony K M, Sepulveda-Jauregui A, Martinez-Cruz K, Bondurant A, Grosse G and Jones M C 2015 Thermokarst lake methanogenesis along a complete talik profile *Biogeosciences* **12** 4317–31

Hoehler T M, Borowski W S, Alperin M J, Rodriguez N M and Paull C K 2000 Model, stable isotope, and radiotracer characterization of anaerobic methane oxidation in gas hydrate-bearing sediments of the Blake Ridge *Proceedings of the Ocean Drilling Program, Scientific Results, Vol. 164* IODP 79–85

Kao-Kniffin J, Woodcroft B J, Carver S M, Bockheim J G, Handelsman J, Tyson G W, Hinkel K M and Mueller C W 2015 Archaeal and bacterial communities across a chronosequence of drained lake basins in arctic alaska *Sci. Rep.* **5** srep18165

Knittel K and Boetius A 2009 Anaerobic oxidation of methane: progress with an unknown process *Annu. Rev. Microbiol.* **63** 311–34

Liptay K, Chanton J, Czepiel P and Mosher B 1998 Use of stable isotopes to determine methane oxidation in landfill cover soils *J. Geophys. Res. Atmospheres* **103** 8243–50

Martin M 2011 Cutadapt removes adapter sequences from high-throughput sequencing reads *EMBnet. Journal* **17** 10–2

Martinez-Cruz K, Leewis M-C, Herriott I C, Sepulveda-Jauregui A, Anthony K W, Thalasso F and Leigh M B 2017 Anaerobic oxidation of methane by aerobic methanotrophs in sub-Arctic lake sediments *Sci. Total Environ.* **607** 23–31

Martinez-Cruz K, Sepulveda-Jauregui A, Walter Anthony K and Thalasso F 2015 Geographic and seasonal variation of dissolved methane and aerobic methane oxidation in Alaskan lakes *Biogeosciences* **12** 4595–606

McCalley C K *et al* 2014 Methane dynamics regulated by microbial community response to permafrost thaw *Nature* **514** 478–81

Michał B., Gagat P., Jabłoński S., Chilimoniuk J., Gaworski M., Mackiewicz P. and Marcin Ł. 2018 PhyMet2: a database and toolkit for phylogenetic and metabolic analyses of methanogens *Env Microbiol Rep* **10** (3) 378-382

Mitzscherling J, Winkel M, Winterfeld M, Horn F, Yang S, Grigoriev M N, Wagner D, Overduin P P and Liebner S 2017 The development of permafrost bacterial communities under submarine conditions *J. Geophys. Res. Biogeosciences* **2017** JG003859

Norði K á, Thamdrup B and Schubert C J 2013 Anaerobic oxidation of methane in an iron-rich Danish freshwater lake sediment *Limnol. Oceanogr.* **58** 546–54

Norði K á and Thamdrup B 2014 Nitrate-dependent anaerobic methane oxidation in a freshwater sediment *Geochim. Cosmochim. Acta* **132** 141–50

Olefeldt D *et al* 2016 Circumpolar distribution and carbon storage of thermokarst landscapes *Nat. Commun.* **7** 13043

Preuss I, Knoblauch C, Gebert J and Pfeiffer E-M 2013 Improved quantification of microbial CH4 oxidation efficiency in arctic wetland soils using carbon isotope fractionation *Biogeosciences* **10** 2539–52

Quast C, Pruesse E, Yilmaz P, Gerken J, Schweer T, Yarza P, Peplies J and Glöckner F O 2012 The SILVA ribosomal RNA gene database project: improved data processing and web-based tools *Nucleic Acids Res.* **41** D590–6

Raghoebarsing A A *et al* 2006 A microbial consortium couples anaerobic methane oxidation to denitrification *Nature* **440** 918–21

Rinke C *et al* 2013 Insights into the phylogeny and coding potential of microbial dark matter *Nature* **499** 431–7

Rivkina E, Petrovskaya L, Vishnivetskaya T, Krivushin K, Shmakova L, Tutukina M, Meyers A and Kondrashov F 2016 Metagenomic analyses of the late Pleistocene permafrost—additional tools for reconstruction of environmental conditions *Biogeosciences* **13** 2207–19

Ruff S E, Biddle J F, Teske A P, Knittel K, Boetius A and Ramette A 2015 Global dispersion and local diversification of the methane seep microbiome *Proc. Natl Acad. Sci.* **112** 4015–20

Ruff S E, Felden J, Gruber-Vodicka H R, Marcon Y, Knittel K, Ramette A and Boetius A 2018 *In situ* development of a methanotrophic microbiome in deep-sea sediments *ISME J.* **13** 197-213

Schneider von Deimling T, Grosse G, Strauss J, Schirrmeister L, Morgenstern A, Schaphoff S, Meinshausen M and Boike J 2015 Observation-based modelling of permafrost carbon fluxes with accounting for deep carbon deposits and thermokarst activity *Biogeosciences* **12** 3469–88

Schubert C J, Vazquez F, Lösekann-Behrens T, Knittel K, Tonolla M and Boetius A 2011 Evidence for anaerobic oxidation of methane in sediments of a freshwater system (Lago di Cadagno) *Fems Microbiol. Ecol.* **76** 26–38

Sepulveda-Jauregui A, Martinez-Cruz K, Strohm A, Walter Anthony K M and Thalasso F 2012 A new method for field measurement of dissolved methane in water using infrared tunable diode laser absorption spectroscopy *Limnol. Oceanogr. Methods* **10** 560–7

Sepulveda-Jauregui A, Walter Anthony K M, Martinez-Cruz K, Greene S and Thalasso F 2015 Methane and carbon dioxide emissions from 40 lakes along a north–south latitudinal transect in Alaska *Biogeosciences* **12** 3197–223

Shcherbakova V., Yoshimura Y., Ryzhmanova Y, Taguchi Y., Segawa T., Oshurkova V., Rivkina E. *et al* 2016 Archaeal communities of Arctic methane-containing permafrost *FEMS Microbial. Ecol.* **92** fiw135

Sorokin D Y *et al* 2017 Discovery of extremely halophilic, methyl-reducing euryarchaea provides insights into the evolutionary origin of methanogenesis *Nat. Microbiol.* **2** nmicrobiol201781

Strauss J *et al* 2017 Deep Yedoma permafrost: a synthesis of depositional characteristics and carbon vulnerability *Earth-Sci. Rev.* **172** 75–86

Strauss J, Schirrmeister L, Grosse G, Wetterich S, Ulrich M, Herzschuh U and Hubberten H-W 2013 The deep permafrost carbon pool of the Yedoma region in Siberia and Alaska *Geophys. Res. Lett.* **40** 2013GL058088

Strauss J, Schirrmeister L, Mangelsdorf K, Eichhorn L, Wetterich S and Herzschuh U 2015 Organic-matter quality of deep permafrost carbon—a study from Arctic Siberia *Biogeosciences* **12** 2227–45

Timmers P H, Suarez-Zuluaga D A, van Rossem M, Diender M, Stams A J and Plugge C M 2015 Anaerobic oxidation of methane associated with sulfate reduction in a natural freshwater gas source *ISME J.* Online **10** 1400–12

Tveit A, Schwacke R, Svenning M M and Urich T 2012 Organic carbon transformations in high-Arctic peat soils: key functions and microorganisms *ISME J* Online **7** 299–311

Vaksmaa A, Jetten M S M, Ettwig K F and Lüke C 2017 McrA primers for the detection and quantification of the anaerobic archaeal methanotroph 'Candidatus Methanoperedens nitroreducens' *Appl. Microbiol. Biotechnol.* **101** 1631–41

Vaksmaa A, Lüke C, van Alen T, Valè G, Lupotto E, Jetten M S M and Ettwig K F 2016 Distribution and activity of the anaerobic methanotrophic community in a nitrogen-fertilized Italian paddy soil *FEMS Microbiol. Ecol.* **92** fiw181

Walter Anthony K, Daanen R, Anthony P, Schneider von Deimling T, Ping C-L, Chanton J P and Grosse G 2016 Methane emissions proportional to permafrost carbon thawed in Arctic lakes since the 1950s *Nat. Geosci.* **9** 679–82

Walter Anthony K M *et al* 2014 A shift of thermokarst lakes from carbon sources to sinks during the Holocene epoch *Nature* **511** 452–6

Walter Anthony K W, von Deimling T S, Nitze I, Frolking S, Emond A, Daanen R, Anthony P, Lindgren P, Jones B and Grosse G 2018 21st-century modeled permafrost carbon emissions accelerated by abrupt thaw beneath lakes *Nat. Commun.* **9** 3262

Walter K M, Smith L C and Chapin F S 2007 Methane bubbling from northern lakes: present and future contributions to the global methane budget *Philos. Trans. R. Soc. -Math. Phys. Eng. Sci.* **365** 1657–76

Walter K M, Zimov S A, Chanton J P, Verbyla D and Chapin F S 2006 Methane bubbling from Siberian thaw lakes as a positive feedback to climate warming *Nature* **443** 71–5

Weber H S, Habicht K S and Thamdrup B 2017 Anaerobic Methanotrophic Archaea of the ANME-2d Cluster Are Active in a Low-sulfate Iron-rich Freshwater Sediment Front. Microbiol. **8** 619

Whiticar M J 1999 Carbon and hydrogen isotope systematics of bacterial formation and oxidation of methane *Chem. Geol.* **161** 291–314

Wik M, Varner R K, Anthony K W, MacIntyre S and Bastviken D 2016 Climate-sensitive northern lakes and ponds are critical components of methane release *Nat. Geosci.* **9** 99–105

Winkel M *et al* 2018 Anaerobic methanotrophic communities thrive in deep submarine permafrost *Sci. Rep.* **8** 1291

Zhang J, Kobert K, Flouri T and Stamatakis A 2014 PEAR: a fast and accurate Illumina Paired-End reAd mergeR *Bioinformatics* **30** 614–20

Zhou J, Bruns M A and Tiedje J M 1996 DNA recovery from soils of diverse composition *Appl. Environ. Microbiol.* **62** 316–22